Incommensurate nematic fluctuations in the two-dimensional Hubbard model

Christoph Husemann and Walter Metzner
Max Planck Institute for Solid State Research, D-70569 Stuttgart, Germany
(Dated: February 26, 2013)

We analyze effective d-wave interactions in the two-dimensional extended Hubbard model at weak coupling and small to moderate doping. The interactions are computed from a renormalization group flow. Attractive d-wave interactions are generated via antiferromagnetic spin fluctuations in the pairing and charge channels. Above Van Hove filling, the d-wave charge interaction is maximal at incommensurate diagonal wave vectors, corresponding to nematic fluctuations with a diagonal modulation. Below Van Hove filling a modulation along the crystal axes can be favored. The nematic fluctuations are enhanced by the nearest-neighbor interaction in the extended Hubbard model, but they always remain smaller than the dominant antiferromagnetic, pairing, or charge density wave fluctuations.

I. INTRODUCTION

Numerous layered correlated electron compounds exhibit competing instabilities, which are driven by a variety of dynamically generated effective interactions. This feature is already borne out by the simplest model of a single layer in such systems, the two-dimensional Hubbard model. Near half-filling, a whole zoo of enhanced fluctuations is generated in that model, not only in the doped Mott insulator regime at strong coupling,[1] but also for a weak bare interaction.[2–6] In addition to the pronounced antiferromagnetic and d-wave superconducting fluctuations, an attractive charge forward scattering interaction with a $d_{x^2-y^2}$-wave symmetry was found.[7,8] If strong enough, such an interaction can trigger a d-wave Pomeranchuk instability leading to a nematic state with broken orientation symmetry.[9]

Nematic order with a $d_{x^2-y^2}$ symmetry has been observed in several layered correlated electron compounds. A nematic phase with a sharp phase boundary has been established in a series of experiments on ultrapure $Sr_3Ru_2O_7$ crystals in a strong magnetic field.[10] Electronic nematicity has also been observed in the high temperature superconductor $YBa_2Cu_3O_y$ in transport experiments[11,12] and neutron scattering.[13]

Nematic tendencies compete with other instabilities. In a functional renormalization group (fRG) analysis, with forward scattering and other interaction channels treated on equal footing, nematic fluctuations in the two-dimensional Hubbard model were found to be weaker than antiferromagnetism and d-wave superconductivity.[14] However, this does not necessarily prevent a nematic state, since nematic order may coexist with antiferromagnetism[15] and superconductivity.[16,17] Moreover, the fRG calculations are reliable only in the weak coupling regime. A pronounced nematicity has been obtained by dynamical cluster mean-field calculations for the two-dimensional Hubbard model at strong coupling.[18]

In a recent analysis of secondary instabilities generated by antiferromagnetic fluctuations in a two-dimensional electron system with a nearly half-filled band, Metlitski and Sachdev[19,20] found a tendency toward formation of a *modulated* nematic state. In that state the nematic order oscillates across the crystal, with generally incommensurate wave vectors that point along the Brillouin zone diagonal and connect antiferromagnetic hot spots with collinear Fermi velocities. At the same wave vectors the bare d-wave polarization function of tight-binding electrons on a square lattice has pronounced peaks, which also indicates that a modulated nematic state is favored over a homogeneous one.[21] Upon reducing the electron concentration the hot spots move toward the saddle points of the dispersion and the modulation vector shrinks, until it vanishes at Van Hove filling. Below Van Hove filling a modulation with a wave vector along the crystal axes can be favored.[21]

In this article we analyze the tendency toward formation of a modulated nematic state in the two-dimensional Hubbard model and its extension with a nearest-neighbor interaction. To this end we compute the effective two-particle interaction from a fRG flow equation and compare the nematic channel to antiferromagnetic, charge density, and pairing interactions. All channels are treated on equal footing and the approximations are controlled at weak coupling. We find that away from Van Hove filling a modulated nematic instability can indeed be favored over a homogeneous one, but remains in any case subleading compared to antiferromagnetism and d-wave superconductivity. The nearest-neighbor interaction present in the extended Hubbard model enhances the nematic fluctuations.

The paper is structured as follows. In Sec. II we introduce the extended Hubbard model and some notation. In Sec. III we describe the fRG flow equation and specify the parametrization of the effective two-particle interaction. Results for the effective interaction are presented and discussed in Sec. IV. A summary with the main conclusions follows in Sec. V.

II. EXTENDED HUBBARD MODEL

We will analyze the extended Hubbard model on a square lattice with a nearest neighbor hopping amplitude $t > 0$ and a next-to-nearest neighbor hopping $t' < 0$. In

standard second quantization notation, the corresponding Hamiltonian reads

$$H = \sum_{\mathbf{k},\sigma} \epsilon_{\mathbf{k}} a^\dagger_{\mathbf{k}\sigma} a_{\mathbf{k}\sigma} + U \sum_j n_{j\uparrow} n_{j\downarrow} + V \sum_{\langle j,j'\rangle} n_j n_{j'} \,, \quad (1)$$

with a tight-binding dispersion of the form $\epsilon_{\mathbf{k}} = -2t(\cos k_x + \cos k_y) - 4t' \cos k_x \cos k_y$. The Hubbard interaction $U > 0$ is an on-site repulsion of electrons with opposite spin. The operator $n_{j\sigma}$ counts electrons with spin orientation σ on the lattice site j, and $n_j = n_{j\uparrow} + n_{j\downarrow}$. The second interaction term with $V > 0$ is a density-density repulsion between nearest neighbor lattice sites. The lattice sum over nearest neighbors $\langle j, j'\rangle$ is defined such that each bond is taken into account only once. The nearest neighbor interaction favors charge order. In mean field theory there is a first order transition between spin and charge density wave order as a function of V.[22,23] We shift the chemical potential μ by $4t'$ such that for $\mu = 0$ the Fermi surface contains the saddle points $(\pi, 0)$ and $(0, \pi)$, where the gradient of $\epsilon_{\mathbf{k}}$ vanishes. The corresponding filling is referred to as Van Hove filling.

In a functional integral formalism, a one-band model of interacting fermions is described by a bare action of the form[24]

$$\mathcal{S}[\Psi] = \int \mathrm{d}k \sum_\sigma \overline{\psi}_\sigma(k)[-ik_0 + (\epsilon_{\mathbf{k}} - \mu)]\psi_\sigma(k) + \mathcal{V}_0[\Psi] \,, \quad (2)$$

with anticommuting Grassmann fields $\overline{\psi}$ and ψ. In addition to momentum $\mathbf{k}$ and spin σ the fields $\overline{\psi}_\sigma(k)$ and $\psi_\sigma(k)$ also depend on Matsubara frequencies k_0. The variable $k = (k_0, \mathbf{k})$ collects frequencies and momenta, and $\int \mathrm{d}k$ is a short-hand notation for $\int \frac{\mathrm{d}k_0}{2\pi} \int \frac{\mathrm{d}^2\mathbf{k}}{(2\pi)^2}$. We consider only the case of temperature zero in this paper, so that the Matsubara sums are integrals. The symbol Ψ denotes a dependence on both ψ and $\overline{\psi}$. For the extended Hubbard model, the bare two-fermion interaction can be written as

$$\mathcal{V}_0[\Psi] = \frac{1}{2} \int \mathrm{d}p_1 \mathrm{d}p_2 \mathrm{d}p_3 \; V_0(\mathbf{p_1}, \mathbf{p_2}, \mathbf{p_3}) \times \sum_{\sigma,\sigma'} \overline{\psi}_\sigma(p_1) \overline{\psi}_{\sigma'}(p_2) \psi_{\sigma'}(p_3) \psi_\sigma(p_4), \quad (3)$$

where $p_4 = p_1 + p_2 - p_3$ is fixed by momentum and frequency conservation, and

$$V_0(\mathbf{p_1}, \mathbf{p_2}, \mathbf{p_3}) = U + V g(\mathbf{p_2} - \mathbf{p_3}), \quad (4)$$

with $g(\mathbf{q}) = 2(\cos q_x + \cos q_y)$.

III. WEAK COUPLING FUNCTIONAL RG

We compute the effective two-particle interaction of the extended Hubbard model from a functional RG flow.[2] To this end we regularize the bare action by introducing a smooth frequency cutoff Λ, corresponding to a regularized bare propagator

$$G_0^\Lambda(k) = \frac{k_0^2}{k_0^2 + \Lambda^2} \frac{1}{ik_0 - \epsilon_{\mathbf{k}} + \mu} \,. \quad (5)$$

The effective interaction $\mathcal{V}^\Lambda$ on scale Λ interpolates smoothly between the bare interaction $\mathcal{V}_0$ at $\Lambda = \infty$ and the final effective two-particle interaction obtained in principle for $\Lambda \to 0$. The exact flow of $\mathcal{V}^\Lambda$ is determined by a differential flow equation, which involves effective m-particle interactions of arbitrary order m.[2] We use a weak-coupling truncation of the exact flow equation, where m-particle contributions with $m \geq 3$ and self-energy feedback to the flow of $\mathcal{V}^\Lambda$ are neglected. Corrections to this approximation are of order $(\mathcal{V}^\Lambda)^3$. The truncated flow equation has the schematic form

$$\frac{d}{d\Lambda} \mathcal{V}^\Lambda = \frac{1}{2} \mathrm{tr} \left(\dot{G}_0^\Lambda \frac{\partial^2 \mathcal{V}^\Lambda}{\partial \Psi^2} G_0^\Lambda \frac{\partial^2 \mathcal{V}^\Lambda}{\partial \Psi^2} \right) , \quad (6)$$

where $\dot{G}_0^\Lambda = \frac{d}{d\Lambda} G_0^\Lambda$. Graphically this corresponds to two vertices connected by two regularized propagators (one differentiated) forming particle-particle or particle-hole bubbles.

We neglect the frequency dependence of the effective interaction, which is irrelevant in power-counting at weak coupling. To obtain an efficient parametrization of the momentum dependence we make an ansatz[25]

$$\mathcal{V}^\Lambda[\Psi] = \mathcal{V}_0[\Psi] + \mathcal{V}_{\mathrm{M}}^\Lambda[\Psi] + \mathcal{V}_{\mathrm{K}}^\Lambda[\Psi] + \mathcal{V}_{\mathrm{D}}^\Lambda[\Psi], \quad (7)$$

which is a decomposition into spin, charge, and pairing channels. The spin or magnetic channel describes the interaction of spin operators

$$\mathcal{V}_{\mathrm{M}}^\Lambda[\Psi] = -\sum_{n=1}^{2} \int \mathrm{d}q \; M_n^\Lambda(\mathbf{q}) \sum_{a=1}^{3} S_n^{(a)}(q) S_n^{(a)}(-q) \quad (8)$$

with $S_n^{(a)}(q) = \frac{1}{2} \int \mathrm{d}k \sum_{\sigma\sigma'} \overline{\psi}_\sigma(k) \tau^{(a)}_{\sigma\sigma'} \psi_{\sigma'}(k+q) f_n(\mathbf{k} + \frac{\mathbf{q}}{2})$. Here $\tau^{(a)}$ are Pauli matrices, and $f_1(\mathbf{k}) = 1$ and $f_2(\mathbf{k}) = \cos k_x - \cos k_y$ are s-wave and d-wave form factors, respectively. The coupling functions $M_n^\Lambda(\mathbf{q})$ evolve in the RG flow. If $M_1^\Lambda(\mathbf{q})$ develops a peak at (close to) $\mathbf{q} = (\pi, \pi)$ which diverges upon lowering Λ, the system tends to (incommensurate) antiferromagnetic order.

A similar parametrization is chosen for the charge channel

$$\mathcal{V}_{\mathrm{K}}^\Lambda[\Psi] = -\frac{1}{4} \sum_{n=1}^{2} \int \mathrm{d}q \; K_n^\Lambda(\mathbf{q}) N_n(q) N_n(-q), \quad (9)$$

where $N_n(q) = \int \mathrm{d}k \sum_\sigma \overline{\psi}_\sigma(k) \psi_\sigma(k+q) f_n(\mathbf{k} + \frac{\mathbf{q}}{2})$ are density operators. An enhancement of $K_1^\Lambda(\mathbf{q})$ at a finite wave vector $\mathbf{q}$ indicates a tendency toward formation of a charge density wave. In this work, we pay particular attention to the coupling function $K_2^\Lambda(\mathbf{q})$ near $\mathbf{q} = 0$, which, if sufficiently large, can drive a d-wave

Pomeranchuk instability leading to a nematic state. At $\mathbf{Q} = (\pi, \pi)$ the coupling $K_2(\mathbf{Q})$ will not be very pronounced, because for $\mathbf{k}$ sitting on a Van Hove point, $\mathbf{k} + \frac{\mathbf{Q}}{2}$ points to a zone diagonal where the form factor f_2 is zero. Note that $\langle N_2(Q)\rangle$ with $Q = (0, \mathbf{Q})$ differs from the familiar d-density wave order parameter[26] $i\langle \int \mathrm{d}k \sum_\sigma \overline{\psi}_\sigma(k)\psi_\sigma(k+Q) f_2(\mathbf{k})\rangle$.

The pairing channel describes the interaction

$$\mathcal{V}_{\mathrm{D}}^{\Lambda}[\Psi] = -\sum_{n=1}^{2} \int \mathrm{d}q \; D_n^{\Lambda}(\mathbf{q}) \overline{X}_n(q) X_n(q) \qquad (10)$$

with spin singlet Cooper pairs

$$\overline{X}(q) = \int \mathrm{d}k \; \overline{\psi}_\uparrow(k)\overline{\psi}_\downarrow(q-k) f_n(\tfrac{\mathbf{q}}{2} - \mathbf{k}) \,,$$
$$X(q) = \int \mathrm{d}k \; \psi_\downarrow(k)\psi_\uparrow(q-k) f_n(\tfrac{\mathbf{q}}{2} - \mathbf{k}) \,.$$

The form factors determine the symmetry of the gap. A diverging (upon lowering Λ) peak of $D_1^\Lambda(\mathbf{q})$ at $\mathbf{q} = 0$ indicates an s-wave pairing instability, and a diverging peak of $D_2^\Lambda(\mathbf{q})$ at $\mathbf{q} = 0$ a d-wave pairing instability, so that a superconducting state is favored. Since both form factors are even functions of momentum we only consider singlets in the spin dependence.

The restriction to s-wave and d-wave form factors in our ansatz is motivated by the dominance of s-wave and d-wave interactions observed in all previous fRG studies of Hubbard-type models in the parameter range considered here.[2]

Substituting the ansatz Eq. (7) into the flow equation generates a variety of different one-loop graphs, not all being of the form of the ansatz. We will use a suitable approximate projection which was developed in Ref. 25. First, the graphs are sorted according to the transfer momentum that propagates through the fermion loop. As long as the coupling functions do not have pronounced peaks this is the main momentum dependence and the graphs can be assigned to one channel. Since the form factors f_1 and f_2 are orthonormal functions on $[-\pi, \pi]^2$, the graphs in each channel can be projected to the flow of coupling functions by integration. The resulting flow equations can be found in Ref. 25 and have been shown to yield a reasonable approximation to the RG flow.

The above truncation of the RG is a weak coupling approximation. For high scales, U/Λ is a small parameter, which allows to truncate at one-loop order. Generically couplings start to grow when the scale is descreased. In an intermediate scale regime there are phase space arguments such that the one-loop flow remains valid although the couplings are not small anymore.[27] Eventually, the coupling functions become too large for certain momenta and the truncation becomes unreliable. We then stop the flow and interpret the rapid growth of the leading coupling as an instability indicating a corresponding ordered state. Specifically, we stop the flow when the maximum of the coupling functions exceeds $V_{\max} = 20t$. The stopping scale Λ_* is an upper bound for the critical scale, at which interactions diverge.

IV. EFFECTIVE D-WAVE INTERACTIONS

We now present results for the effective d-wave interactions in the charge and pairing channel in the presence of strong antiferromagnetic correlations. Throughout this section we choose a relatively weak Hubbard interaction $U = 3t$.

The leading instabilities are signalled by diverging coupling functions in the corresponding channel. The divergence of the full two-particle vertex is well captured by these coupling functions. However, to compare effective interactions quantitatively, one has to sum the contributions from all terms in the decomposition Eq. (7), including also the bare interaction $\mathcal{V}_0$. Contributions from the bare interactions and other channels can be significant in channels where the effective interaction remains bounded.

The complete effective interaction in the various channels can be extracted from the two-particle vertex $\Gamma^\Lambda_{\sigma_1\sigma_2;\sigma_3\sigma_4}(p_1, p_2; p_3, p_4)$, which is the antisymmetrized kernel of $\mathcal{V}^\Lambda$, that is,

$$\mathcal{V}^\Lambda[\Psi] = \frac{1}{4} \sum_{\sigma_1,\ldots,\sigma_4} \int \mathrm{d}p_1 \mathrm{d}p_2 \mathrm{d}p_3 \, \Gamma^\Lambda_{\sigma_1\sigma_2;\sigma_3\sigma_4}(p_1, p_2; p_3, p_4) \times \overline{\psi}_{\sigma_1}(p_1)\overline{\psi}_{\sigma_2}(p_2)\psi_{\sigma_3}(p_3)\psi_{\sigma_4}(p_4) \,, \qquad (11)$$

where $p_4 = p_1 + p_2 - p_3$. We denote the static limit of Γ^Λ by $\Gamma^\Lambda_{\sigma_1\sigma_2;\sigma_3\sigma_4}(\mathbf{p}_1, \mathbf{p}_2; \mathbf{p}_3, \mathbf{p}_4)$. The effective singlet pairing interaction is then given by

$$\Gamma^{\mathrm{SC},\Lambda}_{\mathbf{p}\mathbf{p}'} = \Gamma^\Lambda_{\uparrow\downarrow;\downarrow\uparrow}(\mathbf{p}, -\mathbf{p}; -\mathbf{p}', \mathbf{p}') \,, \qquad (12)$$

and the effective charge interaction by

$$\Gamma^{\mathrm{C},\Lambda}_{\mathbf{p}\mathbf{p}'}(\mathbf{q}) = \frac{1}{4} \sum_{\sigma,\sigma'} \Gamma^\Lambda_{\sigma\sigma';\sigma'\sigma}(\mathbf{p}, \mathbf{p}'; \mathbf{p}' - \mathbf{q}, \mathbf{p} + \mathbf{q}) \,, \qquad (13)$$

where $\mathbf{q}$ is the momentum transfer. In a renormalized mean-field theory of spin singlet superconductivity based on Γ^Λ, only the pairing interaction $\Gamma^{\mathrm{SC},\Lambda}_{\mathbf{p}\mathbf{p}'}$ contributes.[28] Similarly, a renormalized mean-field theory for charge order with a modulation vector $\mathbf{q}$ involves exclusively the charge interaction $\Gamma^{\mathrm{C},\Lambda}_{\mathbf{p}\mathbf{p}'}(\mathbf{q})$.

The s-wave and d-wave components of the interactions are extracted by the projections

$$\gamma_n^{\mathrm{SC},\Lambda} = \int \frac{\mathrm{d}^2\mathbf{p}}{(2\pi)^2} \frac{\mathrm{d}^2\mathbf{p}'}{(2\pi)^2} \, f_n(\mathbf{p}) f_n(\mathbf{p}') \, \Gamma^{\mathrm{SC},\Lambda}_{\mathbf{p}\mathbf{p}'} \qquad (14)$$

and

$$\gamma_n^{\mathrm{C},\Lambda}(\mathbf{q}) = \int \frac{\mathrm{d}^2\mathbf{p}}{(2\pi)^2} \frac{\mathrm{d}^2\mathbf{p}'}{(2\pi)^2} \, f_n(\mathbf{p} + \tfrac{\mathbf{q}}{2}) f_n(\mathbf{p}' - \tfrac{\mathbf{q}}{2}) \, \Gamma^{\mathrm{C},\Lambda}_{\mathbf{p}\mathbf{p}'}(\mathbf{q}) \qquad (15)$$

with $n = 1, 2$. Inserting the channel decomposition Eq. (7), the d-wave components can be written as

$$\gamma_2^{\mathrm{SC},\Lambda} = V - D_2^\Lambda(\underline{0}) + \ldots \,, \qquad (16)$$

and

$$\gamma_2^{\mathrm{C},\Lambda}(\mathbf{q}) = -\frac{V}{2} - \frac{1}{2}K_2^{\Lambda}(\mathbf{q}) + \dots , \qquad (17)$$

where the dots refer to fluctuation contributions from other channels. Complete expressions for $\gamma_n^{\mathrm{SC},\Lambda}$ and $\gamma_n^{\mathrm{C},\Lambda}(\mathbf{q})$ in terms of the bare interaction and the coupling functions M_n^{Λ}, K_n^{Λ} and D_n^{Λ} are given in the Appendix. Note that positive coupling functions yield attractive (negative) contributions to the corresponding effective interactions.

A. Van Hove filling

We first consider the case of Van Hove filling for various choices of $t' < 0$. For $|t'| < 0.237t$ the RG flow runs into an antiferromagnetic instability, that is, $M_1^{\Lambda}(\mathbf{q})$ with $\mathbf{q}$ close to (π,π) reaches $V_{\max}$ first. For $|t'| < 0.11t$ the maximum of $M_1^{\Lambda_*}(\mathbf{q})$ is situated at $\mathbf{Q} = (\pi,\pi)$, while it deviates from (π,π) for larger $|t'|$. However, this shift of $\mathbf{q}$ depends sensitively on the choice of Λ_*, and the maximal value of $M_1^{\Lambda_*}(\mathbf{q})$ differs only very little from its value at $\mathbf{Q}$. For $|t'| > 0.237t$ the dominant instability is d-wave pairing, that is, $D_2^{\Lambda}(\mathbf{0})$ is the largest coupling at Λ_*. The transition from antiferromagnetism to d-wave pairing upon increasing $|t'|$ was found already in the first fRG studies of the two-dimensional Hubbard model.[4,5]

In Fig. 1 we show results for the effective d-wave interactions at the scale Λ_* as a function of t'/t. The antiferromagnetic (AF) and d-wave pairing (dSC) regions are separated by a vertical dashed line. The stopping scale Λ_* decreases monotonically from $0.194t$ at $t' = 0$ to $0.013t$ at $t' = -0.28t$ for $V = 0$, and from $0.162t$ at $t' = 0$ to $0.007t$ at $t' = -0.28t$ for $V = 0.74t$. At Van Hove filling, the d-wave charge interaction $\gamma_2^{\mathrm{C},\Lambda_*}(\mathbf{q})$ is peaked at $\mathbf{q} = \mathbf{0}$. For the plain Hubbard model ($V = 0$) it is always weaker than the d-wave pairing interaction $\gamma_2^{\mathrm{SC},\Lambda_*}$, as observed already in Ref. 14. A finite V enhances the d-wave charge interaction, but it remains small compared to the dominant antiferromagnetic and pairing interactions at small and large $|t'|$, respectively.

In Fig. 2 we plot the effective interactions $\gamma_2^{\mathrm{C},\Lambda_*}(\mathbf{0})$ and $\gamma_2^{\mathrm{SC},\Lambda_*}$ as functions of V at $t' = -0.15t$. From $V = 0$ to $V = 0.758t$ the stopping scale decreases moderately from $\Lambda_* = 0.078t$ to $\Lambda_* = 0.053t$, but it then increases rapidly to $\Lambda_* = 0.656t$ at $V = t$. For increasing $V < 0.758t$, in terms of absolute values, the d-wave interaction in the density channel increases while the d-wave pairing interaction decreases. For $V > 0.758t$ the leading instability changes from incommensurate antiferromagnetism to a charge density wave, that is, the coupling function $K_1^{\Lambda}(\mathbf{Q})$ reaches $V_{\max}$ first and defines the stopping scale Λ_*. The critical value $V = 0.758t$ is close to the mean-field transition point[22] at $V = U/4 = 0.75t$. The drop of $-\gamma_2^{\mathrm{C},\Lambda_*}(\mathbf{0})$ and $-\gamma_2^{\mathrm{SC},\Lambda_*}$ for $V > 0.758t$ is due to a rapidly increasing Λ_* (for increasing V) in the charge density wave regime.

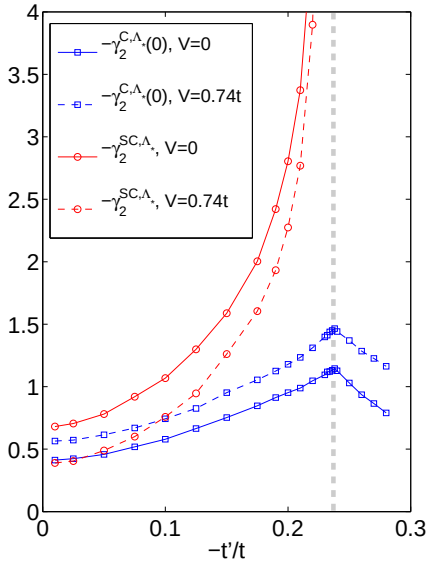

FIG. 1: (Color online) Effective d-wave interactions at the scale Λ_* in units of t as a function of t', for $U = 3t$ at Van Hove filling. The electron density ranges from $n = 1$ at $t' = 0$ to $n = 0.75$ at $t'/t = -0.28$. The pairing interactions $\gamma_2^{\mathrm{SC},\Lambda_*}$ are plotted as circles and charge interactions $\gamma_2^{\mathrm{C},\Lambda_*}(\mathbf{0})$ as squares. Solid lines correspond to $V = 0$ and dashed lines to $V = 0.74t$. In both cases the leading instability changes from antiferromagnetism to d-wave pairing at $t' = -0.237t$ (corresponding to $n = 0.79$).

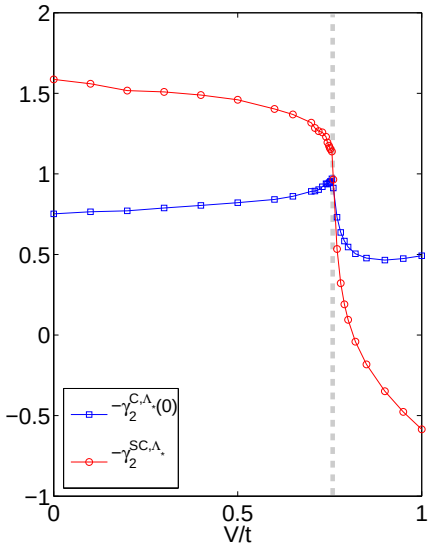

FIG. 2: (Color online) Effective d-wave interactions $\gamma_2^{\mathrm{SC},\Lambda_*}$ (circles) and $\gamma_2^{\mathrm{C},\Lambda_*}(\mathbf{0})$ (squares) in units of t as a function of the nearest-neighbor interaction V, for $t' = -0.15t$ and $U = 3t$ at Van Hove filling ($n = 0.88$). The leading instability changes from incommensurate antiferromagnetism to charge density wave at $V = 0.758t$.

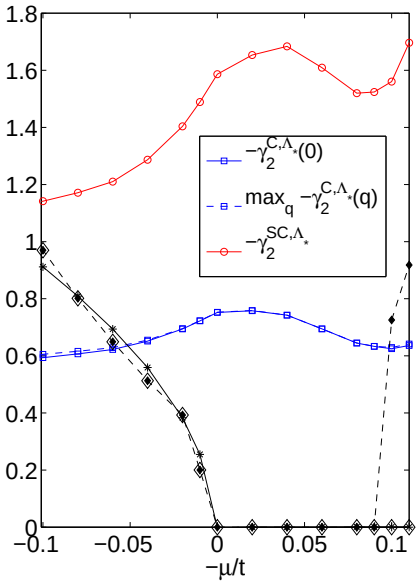

FIG. 3: (Color online) Effective d-wave interactions at the stopping scale Λ_* of antiferromagnetism plotted as functions of μ for $t' = -0.15t$, $U = 3t$, and $V = 0$. The density varies from $n = 0.94$ at $\mu/t = 0.1$ to $n = 0.81$ at $\mu/t = -0.11$. Pairing interactions $\gamma_2^{\mathrm{SC},\Lambda_*}$ are plotted as circles connected by a solid line. The most attractive d-wave charge interactions $\max_{\mathbf{q}} |\gamma_2^{\mathrm{C},\Lambda_*}(\mathbf{q})|$ are plotted as squares connected by a dashed line, while the points corresponding to $\gamma_2^{\mathrm{C},\Lambda_*}(\mathbf{0})$ are connected by a solid line. Also shown are momenta $\mathbf{q}$ where $-\gamma_2^{\mathrm{C},\Lambda_*}(\mathbf{q})$ becomes maximal, with components q_x plotted as open diamonds and q_y as filled diamonds, both connected by a dashed line. Momenta for which the bare d-wave particle-hole bubble $\Phi_{\mathrm{ph}}^{2,\Lambda_*}(\mathbf{q})$ is extremal are shown similarly with components q_x plotted as plus signs and q_y as diagonal crosses. Stars are superpositions of plus signs and crosses for $q_x = q_y$.

B. Away from Van Hove filling

In the following we fix the next-to-nearest neighbor hopping amplitude to $t' = -0.15t$ and vary the chemical potential μ in a limited range around Van Hove filling. For this choice of parameters the RG flow runs into an antiferromagnetic instability, that is, $M_1^{\Lambda}(\mathbf{q})$ with $\mathbf{q}$ close to (π, π) reaches $V_{\max}$ first. For $\mu > 0.03t$ the maximum of $M_1^{\Lambda_*}(\mathbf{q})$ is at $\mathbf{Q} = (\pi, \pi)$, and for $\mu < 0.03t$ four maxima are found at $(\pi, \pi \pm \delta)$ and $(\pi \pm \delta, \pi)$, with δ increasing upon lowering μ. The dominance of antiferromagnetic correlations is not affected by a nearest neighbor interaction V as long as $V < U/4$. At sufficiently low μ (large hole doping), d-wave pairing becomes the leading instability.[3–5] Here we do not enter the d-wave superconducting region.

Results for the effective d-wave interactions $\gamma_2^{\mathrm{SC},\Lambda_*}$ and $\gamma_2^{\mathrm{C},\Lambda_*}$ in the antiferromagnetic background are shown for the plain Hubbard model ($V = 0$) in Fig. 3. We distinguish between $\gamma_2^{\mathrm{SC},\Lambda_*}(\mathbf{0})$ (solid line) and $\max_{\mathbf{q}} |\gamma_2^{\mathrm{C},\Lambda_*}(\mathbf{q})|$ (dashed line). Above Van Hove filling ($\mu > 0$) there are four maxima of $-\gamma_2^{\mathrm{C},\Lambda_*}(\mathbf{q})$ at $\mathbf{q} = (\pm\delta_1, \pm\delta_1)$ with δ_1 decreasing as we approach Van Hove filling. The positions of these maxima are plotted in Fig. 3 as well. They are very close to the positions of the maxima of the static regularized d-wave particle-hole bubble

$$\Phi_{\mathrm{ph}}^{2,\Lambda}(\mathbf{q}) = \int \mathrm{d}p \; G_0^{\Lambda}(p_0, \mathbf{p}) G_0^{\Lambda}(p_0, \mathbf{p} + \mathbf{q}) f_2(\mathbf{p} + \tfrac{\mathbf{q}}{2})^2 \tag{18}$$

at $\Lambda = \Lambda_*$, which are plotted in Fig. 3 for comparison. The small deviations are not significant, that is, they may be due to the limited momentum resolution in the numerics.

A large attraction $\gamma_2^{\mathrm{C},\Lambda_*}(\mathbf{q})$ at a wave vector $\mathbf{q} \neq \mathbf{0}$ would signal a tendency to form a modulated nematic order with a modulation vector $\mathbf{q}$. Such a tendency was found in a recent analysis of secondary instabilities generated by antiferromagnetic fluctuations in a two-dimensional metal by Metlitski and Sachdev.[19,20] The modulation vectors $\mathbf{q}$ are fixed by the position of the antiferromagnetic hot spots, where the antiferromagnetic fluctuations couple most strongly to the electronic excitations near the Fermi surface. Subsequently it was shown that the same modulation vectors $\mathbf{q} = (\pm\delta_1, \pm\delta_1)$ emerge as the momenta where the static d-wave particle-hole bubble is maximal.[21] For a tight-binding dispersion with hopping amplitudes t and t', the modulation is given by[21]

$$\delta_1 = 2 \arccos \sqrt{1 - \frac{\mu}{4|t'|}} \, . \tag{19}$$

Note that $\mu \geq 0$ has been shifted by $4t'$ such that Van Hove filling corresponds to $\mu = 0$. The maxima of the d-wave interaction $-\gamma_2^{\mathrm{C},\Lambda_*}(\mathbf{q})$ obtained from the fRG flow above Van Hove filling are also situated at diagonal momenta of the form $\mathbf{q} = (\pm\delta_1, \pm\delta_1)$, with δ_1 given by Eq. (19) within the numerical resolution. In agreement with Metlitski and Sachdev[19,20] we find that in the antiferromagnetic regime the d-wave density interaction is of the same order of magnitude but smaller than the d-wave pairing interaction. However, while d-wave pairing competes with antiferromagnetism at larger doping, the d-wave density interaction remains rather small.

Slightly below Van Hove filling the particle-hole bubble is very flat. In the numerical solution of the RG flow we find the maximum of $-\gamma_2^{\mathrm{C},\Lambda_*}(\mathbf{q})$ at $\mathbf{q} = 0$ for $-0.08t < \mu < 0$. For lower electron filling, $\mu < -0.08t$, there are again four degenerate maxima, but now at momenta along the crystal axes $(0, \pm\delta_2)$ and $(\pm\delta_2, 0)$. Overall, the strength of the effective d-wave interaction in the density channel is weaker than in the d-wave pairing channel and is maximal around Van Hove filling.

A nearest neighbor repulsion is expected to enhance the d-wave charge correlations. Indeed, in a mean-field study restricted to spatially homogeneous solutions it was

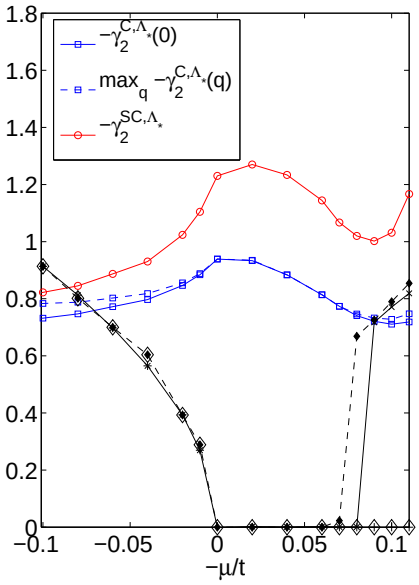

FIG. 4: (Color online) Effective d-wave interactions and modulation vectors as in Fig. 3, but for a finite nearest neighbor interaction $V = 0.74t$.

found that the nearest neighbor interaction in the extended Hubbard model can generate a nematic state.[29]

In Fig. 4 we show results for the effective d-wave interactions for the extended Hubbard model with a finite nearest-neighbor interaction $V = 0.74t$. The other parameters are the same as in Fig. 3. The d-wave density interaction is enhanced by the presence of V, while the pairing interaction is reduced compared to the case $V = 0$. The favorite nematic modulation vectors are not affected significantly by V, but the peaks of $\gamma_2^{C,\Lambda_*}(\mathbf{q})$ at those wave vectors are more pronounced in Fig. 4 compared to the case $V = 0$ plotted in Fig. 3. The stopping scale Λ_* decreases monotonically from $0.105t$ at $\mu/t = 0.1$ to $0.036t$ at $\mu/t = -0.11$ for $V = 0$ (Fig. 3), and from $0.076t$ at $\mu/t = 0.1$ to $0.019t$ at $\mu/t = -0.11$ for $V = 0.74t$ (Fig. 4).

We focused on the case of small or moderate doping. Further away from half-filling, modulated *ferromagnetic* fluctuations with incommensurate wave vectors have been found in mean-field and functional RG studies of the two-dimensional Hubbard model.[30–32]

C. Mechanism

To gain some analytical understanding of the above results, we now discuss the structure of the flow equations for the effective d-wave couplings. The flow equation for the d-wave coupling in the density channel can be written as[25]

$$\frac{d}{d\Lambda}K_2^\Lambda(\mathbf{q}) = -\frac{d\Phi_{\rm ph}^{2,\Lambda}(\mathbf{q})}{d\Lambda}\left[K_2^\Lambda(\mathbf{q}) + V - \alpha_K^\Lambda\right]^2 + F_K^\Lambda(\mathbf{q}), \tag{20}$$

where α_K^Λ is a contribution from s-wave channels given by

$$\alpha_K^\Lambda = \frac{1}{4}\int \frac{\mathrm{d}^2\mathbf{k}}{(2\pi)^2}(\cos k_x + \cos k_y) \times \left[-2D_1^\Lambda(\mathbf{k}) + 3M_1^\Lambda(\mathbf{k}) + K_1^\Lambda(\mathbf{k})\right]. \tag{21}$$

The function $F_K^\Lambda(\mathbf{q})$ originates from d-wave couplings D_2^Λ, M_2^Λ, and K_2^Λ. We do not write this function here,[25] but it was taken into account in our numerical solution of the flow equations. As long as the d-wave interactions are small, contributions from $F_K^\Lambda(\mathbf{q})$ are negligible. Then the only momentum dependence is generated by a scale derivative of the regularized d-wave particle-hole bubble Eq. (18). The initial condition at a high scale Λ_0, derived from second order perturbation theory, is also given by this bubble $K_2^{\Lambda_0}(\mathbf{q}) = -V^2\Phi_{\rm ph}^{2,\Lambda_0}(\mathbf{q}) > 0$. This makes plausible why the maxima of $K_2^\Lambda(\mathbf{q})$ and $-\gamma_2^{C,\Lambda}(\mathbf{q})$ are given by the extrema of the regularized particle-hole bubble.

Even if there is no d-wave coupling initially (for $V = 0$), K_2^Λ is generated in the flow similarly to the mechanism that generates an attraction leading to d-wave pairing. Close to an antiferromagnetic instability the magnetic coupling function obeys $M_1^\Lambda(\mathbf{Q}) \gg M_1^\Lambda(\mathbf{0})$ with $\mathbf{Q} = (\pi, \pi)$. Via integration with the cosine this leads to a sizeable negative contribution in Eq. (21). Then the square bracket in Eq. (20) remains non-zero for $K_2^\Lambda > 0$ and increases with the latter. Since $\partial_\Lambda\Phi_{\rm ph}^{2,\Lambda}(\mathbf{q}) > 0$ and the scale Λ decreases, the coupling function $K_2^\Lambda(\mathbf{q})$ builds up in the flow. It is not essential whether $M_1^\Lambda(\mathbf{k})$ is maximal at or close to (π, π). The modulation of the d-wave coupling is not tied to an incommensurability in the magnetic interactions.

In the same way K_2^Λ is generated by the density channel if $K_1^\Lambda(\mathbf{Q}) \gg K_1^\Lambda(\mathbf{0})$, that is, if the system is close to a charge density wave instability (CDW). The latter is the case for larger V, which also helps to generate K_2^Λ via the constant V in Eq. (20) and via a larger initial condition. Therefore we find a larger effective d-wave interaction in the density channel if the nearest neighbor interaction V is increased, as in Figs. 2 and 4.

The flow equation for D_2^Λ is given by[25]

$$\frac{d}{d\Lambda}D_2^\Lambda(\mathbf{q}) = \frac{d\Phi_{\rm pp}^{2,\Lambda}(\mathbf{q})}{d\Lambda}\left[D_2^\Lambda(\mathbf{q}) - V - \alpha_D^\Lambda\right]^2 + F_D^\Lambda(\mathbf{q}), \tag{22}$$

where $\Phi_{\rm pp}^{2,\Lambda}(\mathbf{q}) = \int \mathrm{d}p\, G_0^\Lambda(p_0, \mathbf{p})G_0^\Lambda(-p_0, \mathbf{q}-\mathbf{p})f_2(\frac{\mathbf{q}}{2}-\mathbf{p})^2$ is the static regularized particle-particle bubble with d-

wave form factors and

$$\alpha_D^\Lambda = \frac{1}{4}\int \frac{\mathrm{d}^2\mathbf{k}}{(2\pi)^2}\,(\cos k_x + \cos k_y)\left[3M_1^\Lambda(\mathbf{k}) - K_1^\Lambda(\mathbf{k})\right]\,. \tag{23}$$

Again we neglect the function $F_D^\Lambda(\mathbf{q})$ for simplicity, which is justified for small K_2^Λ and M_2^Λ. The initial condition at a high scale Λ_0, obtained from second order perturbation theory, is given by $D_2^{\Lambda_0}(\mathbf{q}) = V^2\Phi_{\mathrm{pp}}^{2,\Lambda}(\mathbf{q}) > 0$ and is dominated by the constant $-V$ in Eq. (22). Because $\partial_\Lambda\Phi_{\mathrm{pp}}^{2,\Lambda}(\mathbf{0}) < 0$ and Λ decreases, the coupling $D_2^\Lambda(\mathbf{0})$ would saturate at V if $\alpha_D^\Lambda = 0$. The d-wave pairing can only become large if α_D^Λ is negative. Like for K_2^Λ this is the case in an antiferromagnetic background, which is the main mechanism for d-wave superconductivity in the Hubbard model. However, because of the minus sign in front of $K_1^\Lambda(\mathbf{k})$ in Eq. (23), the vicinity of charge density order is counterproductive for the evolution of d-wave pairing.

It is instructive to compare the contribution from magnetic interactions to the generation of d-wave couplings described above to the hot spot mechanism discovered by Metlitski and Sachdev.[19,20] They consider the situation at a quantum critical point on the phase boundary of a commensurate antiferromagnetic ground state. As a consequence, their spin fluctuation propagator is strongly peaked at (π,π), and electronic excitations around hot spots dominate. The nematic modulation vector is determined by the distance between hot spots with collinear Fermi velocities. Metlitski and Sachdev find a degeneracy between the d-wave couplings in the pairing and charge channels, which is broken only by the Fermi surface curvature. This degeneracy is present also in our flow equations Eqs. (21) and (23), where $M_1^\Lambda(\mathbf{k})$ contributes exactly equally to α_K^Λ and α_D^Λ. The Fermi surface curvature lifts the degeneracy because it reduces the size of the particle-hole bubble at the nematic modulation vector compared to the particle-particle bubble at $\mathbf{q} = \underline{0}$. Singular self-energy contributions at the quantum critical point suppress the curvature effects, so that the nematic correlations are more pronounced than away from criticality.[19]

V. CONCLUSION

We computed effective d-wave interactions in the two-dimensional extended Hubbard model at small to moderate distance from half-filling by using a functional renormalization group flow. In addition to the well-known attraction in the d-wave pairing channel, an attractive interaction in the d-wave charge channel is generated, in agreement with early fRG calculations.[7] If strong enough, that interaction could induce a d-wave Pomeranchuk instability leading to nematic order. However, in comparison to the dominating antiferromagnetism and d-wave pairing, the d-wave charge interaction is found to be relatively weak. It becomes most pronounced at Van Hove filling and can be enhanced by a nearest neighbor interaction V.

The d-wave charge attraction is not necessarily maximal at $\mathbf{q} = 0$. Above Van Hove filling, we find four degenerate peaks of $\gamma_2^{\mathrm{C},\Lambda}(\mathbf{q})$ at diagonal wave vectors $\mathbf{q} = (\pm\delta_1, \pm\delta_1)$ connecting hot spots with collinear Fermi velocities, corresponding to the modulated nematic correlations discovered by Metlitski and Sachdev.[19,20] In the fRG calculation, the peaks are essentially determined by the structure of the d-wave particle-hole bubble, discussed in detail in Ref. 21. Below but close to Van Hove filling $|\gamma_2^{\mathrm{C},\Lambda}(\mathbf{q})|$ is quite flat with a shallow maximum at $\mathbf{q} = 0$. Further decreasing μ one obtains maxima along the crystal axes, again corresponding to extrema in the d-wave bubble.

In any case, the nematic fluctuations in the weakly interacting extended Hubbard model seem to be generically small compared to the dominant channels, which, depending on parameters, are antiferromagnetic, d-wave pairing, or charge density fluctuations at small or moderate doping. The nematic tendency observed experimentally in cuprates is thus probably a strong coupling phenomenon,[15,18] possibly associated with antiferromagnetic quantum criticality.[19,20] For a microscopic theory of the nematic order in $Sr_3Ru_2O_7$ a multi-band model[33] seems to be required.

Acknowledgments

We are grateful to T. Holder, A. Katanin, M. Metlitski, and H. Yamase for valuable discussions.

Appendix A: Expressions for effective interactions

In this appendix we present explicit expressions for the s-wave and d-wave components of the effective charge and pairing interactions in terms of the bare interaction and the coupling functions.

The s-wave component of the effective interaction in the singlet pairing channel as defined in Eq. (14) can be written as

$$\gamma_1^{\mathrm{SC},\Lambda} = U - D_1^\Lambda(\mathbf{0}) + \frac{1}{2}\sum_{n=1,2}\int \frac{\mathrm{d}^2\mathbf{k}}{(2\pi)^2}\left[3M_n^\Lambda(\mathbf{k}) - K_n^\Lambda(\mathbf{k})\right]. \tag{A1}$$

Similarly, the d-wave component is given by

$$\gamma_2^{\mathrm{SC},\Lambda} = V - D_2^\Lambda(\mathbf{0}) + \alpha_D^\Lambda + \frac{1}{2}\int \frac{\mathrm{d}^2\mathbf{k}}{(2\pi)^2}\left[\tfrac{1}{4} + h_1(\mathbf{k}) + h_2(\mathbf{k})\right] \times \left[3M_2^\Lambda(\mathbf{k}) - K_2^\Lambda(\mathbf{k})\right], \tag{A2}$$

with α_D^Λ from Eq. (23). The functions h_n are defined as $h_1(\mathbf{k}) = \frac{1}{2}(\cos k_x + \cos k_y)$ and $h_2(\mathbf{k}) = \cos\frac{k_x}{2}\cos\frac{k_y}{2}$. The

first line is the main contribution and its square enters the flow equation of the coupling function D_2^Λ in Eq. (22).

In the charge channel we allow for a finite transfer momentum $\mathbf{q}$ in the effective interaction between density pairs. Its s-wave component reads

$$\gamma_1^{\mathrm{C},\Lambda}(\mathbf{q}) = \frac{1}{2}U + Vg(\mathbf{q}) - \frac{1}{2}K_1^\Lambda(\mathbf{q}) + a_{1,1}^{\mathrm{C},\Lambda} + a_{1,2}^{\mathrm{C},\Lambda} h_1(\mathbf{q})\,, \tag{A3}$$

where

$$a_{1,n}^{\mathrm{C},\Lambda} = \frac{1}{4}\int \frac{\mathrm{d}^2\mathbf{k}}{(2\pi)^2}\,\Big[-2D_n^\Lambda(\mathbf{k}) + 3M_n^\Lambda(\mathbf{k}) + K_n^\Lambda(\mathbf{k})\Big]\,. \tag{A4}$$

The d-wave component is given by

$$\gamma_2^{\mathrm{C},\Lambda}(\mathbf{q}) = -\frac{1}{2}V - \frac{1}{2}K_2^\Lambda(\mathbf{q}) + \frac{1}{2}\alpha_K^\Lambda + A_2^{\mathrm{C},\Lambda}(\mathbf{q})\,, \tag{A5}$$

with α_K^Λ from Eq. (21). The first three terms enter the flow equation for K_2^Λ, see Eq. (20). The remaining terms are subleading and are given by

$$A_2^{\mathrm{C},\Lambda}(\mathbf{q}) = a_{2,1}^{\mathrm{C},\Lambda} h_1(\mathbf{q}) + a_{2,2}^{\mathrm{C},\Lambda}\cos\frac{q_x}{2}\cos\frac{q_y}{2} + \frac{1}{16}a_{1,2}^{\mathrm{C},\Lambda} \tag{A6}$$

with

$$a_{2,n}^{\mathrm{C},\Lambda} = \frac{1}{4}\int \frac{\mathrm{d}^2\mathbf{k}}{(2\pi)^2}\,h_n(\mathbf{k}) \times\Big[-2D_2^\Lambda(\mathbf{k}) + 3M_2^\Lambda(\mathbf{k}) + K_2^\Lambda(\mathbf{k})\Big]\,. \tag{A7}$$

[1] P. A. Lee, N. Nagaosa, and X. G. Wen, Rev. Mod. Phys. **78**, 17 (2006).
[2] W. Metzner, M. Salmhofer, C. Honerkamp, V. Meden, and K. Schönhammer, Rev. Mod. Phys. **84**, 299 (2012).
[3] D. Zanchi and H. J. Schulz, Phys. Rev. B **61**, 13609 (2000).
[4] C. J. Halboth and W. Metzner, Phys. Rev. B **61**, 7364 (2000).
[5] C. Honerkamp, M. Salmhofer, N. Furukawa, and T. M. Rice, Phys. Rev. B **63**, 035109 (2001).
[6] For a weak coupling analysis of fluctuations in *extended* Hubbard models see, for example, A. P. Kampf and A. A. Katanin, Phys. Rev. B **67**, 125104 (2003).
[7] C. J. Halboth and W. Metzner, Phys. Rev. Lett. **85**, 5162 (2000).
[8] The d-wave attraction in the charge forward scattering channel persists in the strong coupling limit of the Hubbard model, corresponding to the t-J model, see H. Yamase and H. Kohno, J. Phys. Soc. Jpn. **69**, 332 (2000); ibid. **69**, 2151 (2000).
[9] E. Fradkin, S. A. Kivelson, M. J. Lawler, J. P. Eisenstein, and A. P. Mackenzie, Annu. Rev. Condens. Matter Phys. **1**, 153 (2010).
[10] S. A. Grigera et al., Science **306**, 1154 (2004); R. A. Borzi et al., Science **315**, 214 (2007); A. W. Rost et al., Science **325**, 1360 (2009).
[11] Y. Ando et al., Phys. Rev. Lett. **88**, 137005 (2002);
[12] R. Daou et al., Nature (London) **463**, 519 (2010).
[13] V. Hinkov et al., Nature (London) **430**, 650 (2004); V. Hinkov et al., Science **319**, 597 (2008).
[14] C. Honerkamp, M Salmhofer, and T. M. Rice, Eur. Phys. J. B **27**, 127 (2002).
[15] S. A. Kivelson, E. Fradkin, and V. J. Emery, Nature (London) **393**, 550 (1998).
[16] A. Neumayr and W. Metzner, Phys. Rev. B **67**, 035112 (2003).
[17] H. Yamase and W. Metzner, Phys. Rev. B **75**, 155117 (2007).
[18] S. Okamoto, D. Sénéchal, M. Civelli, and A.-M. S. Tremblay, Phys. Rev. B **82**, 180511 (2010).
[19] M. A. Metlitski and S. Sachdev, Phys. Rev. B **82**, 075128 (2010).
[20] M. A. Metlitski and S. Sachdev, New J. Phys. **12**, 105007 (2010).
[21] T. Holder and W. Metzner, arXiv:1202.0497.
[22] M. Murakami, J. Phys. Soc. Jpn. **69**, 1113 (2000).
[23] Y. Zhang and J. Callaway, Phys. Rev. B **39**, 9397 (1989).
[24] J. W. Negele and H. Orland, *Quantum Many-Particle Systems* (Addison-Wesley, Reading, 1987).
[25] C. Husemann and M. Salmhofer, Phys. Rev. B **79**, 195125 (2009).
[26] S. Chakravarty, R. B. Laughlin, D. K. Morr, and C. Nayak, Phys. Rev. B **63**, 094503 (2001)
[27] M. Salmhofer and C. Honerkamp, Prog. Theor. Phys. **105**, 1 (2001).
[28] J. Reiss, D. Rohe, and W. Metzner, Phys. Rev. B **75**, 075110 (2007).
[29] B. Valenzuela and M. A. H. Vozmediano, Phys. Rev. B **63**, 153103 (2001).
[30] P. A. Igoshev, M. A. Timirgazin, A. A. Katanin, A. K. Arzhnikov, and V. Yu. Irkhin, Phys. Rev. B **81**, 094407 (2010).
[31] P. A. Igoshev, V. Yu. Irkhin, and A. A. Katanin, Phys. Rev. B **83**, 245118 (2011).
[32] A. A. Katanin, H. Yamase, and V. Yu. Irkhin, J. Phys. Soc. Jpn. **80**, 063702 (2011).
[33] S. Raghu, A. Paramekanti, E. A. Kim, R. A. Borzi, S. A. Grigera, A. P. Mackenzie, and S. A. Kivelson, Phys. Rev. B **79**, 214402 (2009).